AD-A115 512   AIR FORCE INST OF TECH WRIGHT-PATTERSON AFB OH SCHOO--ETC F/G 18/3
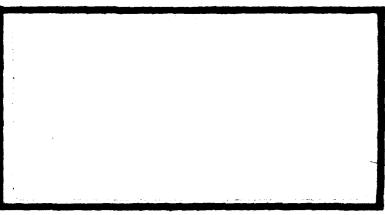   NEUTRON DECAY ELECTRON INJECTION INTO THE MAGNETOSPHERE.(U)
                MAR 82 B L HANSON
UNCLASSIFIED   AFIT/GNE/PH/82-8   NL

END
DATE
FILMED
-7-82
DTIC

DEPARTMENT OF THE AIR FORCE

AIR UNIVERSITY (ATC)

AIR FORCE INSTITUTE OF TECHNOLOGY

Wright-Patterson Air Force Base, Ohio

82 06 14 181

NEUTRON DECAY ELECTRON

INJECTION INTO THE MAGNETOSPHERE

THESIS

AFIT/GNE/PH/82-8   Brian L. Hanson
                                         1st Lt   USAF

Approved for public release; distribution unlimited

NEUTRON DECAY ELECTRON
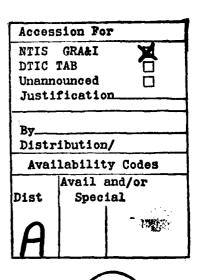
INJECTION INTO THE MAGNETOSPHERE

THESIS

Presented to the Faculty of the School of Engineering

of the Air Force Institute of Technology

Air University

in Partial Fulfillment of the

Requirements for the Degree of

Master of Science

by

Brian L. Hanson, B.S.

1st Lt   USAF

Graduate Nuclear Engineering

March 1982

Acknowledgments

Dr. Joseph Janni of the Air Force Weapons Laboratory proposed this topic. I am deeply indebted to him for supplying me with his support throughout the efforts of this project.

Sincere gratitude is also due to Dr. Robert C. Backstrom at Sandia National Laboratory and Captain Robert J. Greaves of the Air Force Weapons Laboratory for their invaluable support and insights provided in our numerous discussions.

A very strong debt of gratitude is also owed to my faculty advisors, Major Robert N. Davie, Jr., Dr. Charles J. Bridgman, and Major James J. Lange. Their willingness to help when I needed it and to let me work independently at other times was greatly appreciated.

Contents

List of Figures

List of Tables

Abstract

A model to determine magnetospheric electron fluxes from bomb neutron decay is presented. The source of electrons was determined from a neutron decay model dependent on a 37 group neutron spectrum of a nuclear detonation. Monte-carlo simulation of the decay process determined the electron energy and angular spectra as a function of neutron energy. The Air Force Weapons Laboratory's PROMPT code generates neutron spectra from a nuclear detonation at an observer. Using this neutron spectrum and the electron energy and angular distributions from neutron decay theory, an algorithm was developed to calculate the electron flux. An example of a 1 kt burst at 20 km shows that fluxes above normal background can be observed as far away as 400 km. Higher bursts or bursts of larger magnitude will produce higher fluxes at this distance. It is thus concluded that neutron decay alone can generate significant numbers of energetic electrons in the magnetosphere. Their effect may prove to be of tactical significance in medium to high altitude burst scenarios where fission debris is a less significant source of electrons.

Chapter I

Introduction

High altitude nuclear bursts can inject large numbers of high energy electrons and protons into the magnetosphere. These particles can become trapped in the magnetic field and enhance the existing radiation belts. Satellites passing through these belts can be damaged when the radiation is severe enough to penetrate the shielding and reach the large scale integrated circuitry which has a relatively low radiation damage threshold (Ref 1:1). Satellites can be damaged by the lower energy electrons from surface charging in the satellite dielectrics. Because satellites are expensive and serve many important peacetime and wartime missions, satellite survivability and vulnerability concerns both private industry and the government.

This study considers the electrons from bomb neutron decay independent from all other electron sources. Generally, the most significant source of electrons from nuclear bursts is the beta decay of the radioactive fission debris nuclei (Ref 2). However, another source of electrons is from bomb neutron decay. Although neutron decay creates significantly higher electron fluxes than the normal background, this source is often relatively insignificant compared with the electron fluxes from the fission debris (Ref 3:159, 4:4637). But cases do exist where early time electron fluxes are high and cannot be explained by the fission debris source (Ref 5:5). Also

cases exist where the atmosphere severely attenuates the fission debris while the neutrons are much less attenuated. The specific purpose of this research was to model neutron decay electron injection into the terrestrial magnetosphere from nuclear bursts.

This was done to supplement the Air Force Weapon Laboratory's (AFWL) capability to calculate electron environments in the magnetosphere. A prompt radiation computer code existing at AFWL calculates the neutron, gamma, and x-ray spectra from a given nuclear detonation observed at an arbitrary point above the horizon. These spectra are applied to satellite survivability/vulnerability analysis, but they lacked the electron spectrum injected by the decaying neutrons. Such an injection model was formulated and added to AFWL's PROMPT radiation code.

The procedure to investigate this problem involves both the energy and the angular electron distributions from neutron decay. Using monte-carlo techniques to model the decay process, the electron energy and angular distributions were determined as a function of neutron energy. These distributions were added as subroutines to AFWL's PROMPT computer code to calculate the electron flux from arbitrary bomb neutron spectra. To validate the model, a test case compared the theoretical results with Explorer IV satellite data for the Teak event, data that could not be explained by fission debris decay. Other validation tests compared the theoretical results with the zero mass integral and spherical divergence approximations. Finally, the dependence between mass integral and electron flux was related to the effect of different altitude bursts on the electron flux seen by a satellite.

2

Chapter II

Background

Nuclear bursts produce about 10^{23} neutrons per kiloton of fission
yield. These neutrons can interact with the atmosphere, scattering
until they are absorbed. Until they are absorbed, they have a
finite probability of decaying into an electron, proton, and anti-
neutrino. Neutrons have a half life of 10.6 minutes (Ref 6), and
decay according to equation 1,

$$N = \frac{S}{4\pi R^2 \, v_n \tau_n} \tag{1}$$

where N is the number of neutrons that decay per unit volume,
S is the number of neutrons from the source, R is the distance from
the burst, v_n is the neutron velocity, and τ_n is the mean neutron
lifetime.

The atmosphere readily absorbs most neutrons and makes
neutron decay a minor source of electrons deep in the
atmosphere. However, where the atmosphere is thin enough to propa-
gate neutrons, neutron decay can become a significant contributor to
the electron environment (Ref 3:159, 4:4637).

In most electron trapping studies, the radioactive fission
debris nuclei are considered the primary source of electrons. For
most applications this assumption is correct, because neutron decay
produces only one electron, while fission debris decay produces about

3

seven electrons (Ref 2). But the actual relative significance will be a trade-off between the fission fragment and the neutron decay electron production.

In 1962, Killeen, Hess, and Lingenfelter estimated the electron fluxes caused by neutron decay (Ref 4). They concluded that from Starfish, a 1.4 megaton burst at 400 km, the expected electron flux from neutron decay would be less than 10^7 electrons/cm^2-sec near the explosion. This flux is a small fraction of the observed electron flux (Ref 4:3467). However, in reference to this article, Hess later said that this electron flux is not negligible, but is concealed by the considerably larger flux of fission debris electrons from Starfish (Ref 3:159).

More recently, this author estimated the electron flux from neutron decay as a function of distance from a burst. Although the ideal situation of free space and monoenergetic neutrons was examined, it showed that under these conditions, neutron decay contributes significant electron fluxes above normal synchronous background at great distances from a deep space burst (see Appendix A). The normal background at synchronous orbit is about 10^6 electrons/cm^2-sec (Ref 7), and calculations showed that a one megaton burst in free space could generate this flux over 1,000 km from the point of burst.

In reference to these high fluxes, bursts like Teak (75 km) and Orange (45 km) should provide some observational data since the air density is larger than that for Starfish (400 km), but low enough to propagate neutrons (Ref 8). Observation of electron densities of 4.3×10^4 e$^-$/cm^2 (Ref 5:10) were observed by the Explorer IV satellite only 18 minutes after the Teak detonation. The spectrum of the

electron energies was not characteristic of fission debris (Ref 5:5), and an explanation has not been published to this date. Some people postulate that the fluxes could be from protons.

Explorer IV had 3 electron detectors, E>580 keV, E>1 MeV, and E>5 MeV. These energy groups do not provide an ideal spectrum for confirming or denying the neutron decay source, however, the observed flux peak for E<1 MeV is consistent with a neutron decay electron spectrum. AFWL supported this study to better quantify the neutron decay source in terms of magnitude, energy spectra, and spatial distribution as a function of burst yield, location, and observation point.

Chapter III

The Beta Spectrum from Neutron Decay

Electron flux in the exosphere is a time dependent phenomenon
depending on the trapped electron distribution. The trapped elec-
tron distribution depends on the electron motion in the magnetosphere.
Since charged particle motion in a magnetic field depends on the
particle energy and the angle between its velocity vector and the
magnetic field line, these two parameters needed to be investigated.
Since no adequate theoretical model to describe neutron beta decay was
available, data was obtained from monte-carlo simulation of neutron
beta decay. This chapter is broken into three sections. The sec-
tions present the monte-carlo data generation, the resulting energy
distribution, and the resulting angular distribution.

Monte-Carlo Data Generation

No adequate theories exist to accurately describe the electron
energy and angular distributions from neutron decay. Some beta
spectra of thermal neutron decay are available, but theories do not
accurately predict the lower energy regions. Without an acceptable
theory to build a mathematical model, a monte-carlo simulation
of the neutron decay phenomenon was used to generate a data base
for analysis.

The simulation was based on energy and angular probability
functions for specific neutron energies. A beta spectrum of thermal

6

neutrons measured in 1951 by Robson (Ref 9:352) was fit with a fourth
order polynomial of electron energy in keV. This curve was normal-
ized and integrated so that random numbers could be used to specify
decay energies. Electron energy groups of 50 keV each from 0 to
1.15 MeV were used to accumulate energy spectra histories. Electron
spectra from 37 neutron energy groups were generated assuming that
the electrons were isotropic and that the electron originated with
the same velocity as the neutron.

Using relativistic velocity addition and randomly simulated
isotropic electron decay in the center of mass reference frame, the
simulation calculated the electron spectral and angular data for
specified neutron energies. 20,000 histories were sufficient to
calculate energy distributions with standard deviations ($\sqrt{N}/N$) on the
order of 10^{-3} for an average group.

The angular distribution simulation assumed isotropic scatter,
so a two dimensional geometry was used to take advantage of symmetry.
The x-axis was the direction of the neutron velocity vector and the
y-axis was perpendicular to the x-axis. Realizing that the angular
distribution relies on the third dimension, the probability of an
electron emitting at an angle θ above or below the x-axis is

$$P(\theta) = \frac{1-\cos\theta}{2}$$

where θ is defined from 0 to π. This is the distribution function
used to randomly generate θ in the center of mass reference frame.

Once theta was generated, the electron energy was randomly
generated. The combination of this angle and energy was then added

7

relativistically to the neutron velocity to determine the lab frame electron energy and angle distributions. The data was tabulated in electron energy groups of 50 keV each and in angular groups of 5 degrees each.

The resulting angular information depended on neutron energy as well as electron energy. Therefore, for every 50 keV electron energy group, the angular information was divided into 38 angular groups. To account for the increased number of data groups, the iterations were increased to 500,000 histories to get a standard deviation of 10^{-3}.

The monte-carlo simulation was validated by comparing two neutron energy extremes to the original data. A zero energy neutron case was tested and generated the same distribution that was input. A 20 MeV neutron case generated an angular spectrum skewed in the forward direction and a considerably higher energy skewed electron spectrum. Runs using other sets of random numbers were examined and observed deviations were within expected random error.

Polynomial curve fits, based on the monte-carlo data, were then used to save computer space and time during parametric studies. Each set of data for the electron energy spectrum was curve fit by a fourth order polynomial equation in electron energy in keV. Each set of data for the angular distribution was curve fit using a fourth order polynomial equation in theta in radians. The following sections describe each topic in greater detail.

Electron Energy Distribution from Neutron Decay

To determine the electron flux, the electron velocity must be known. Electron velocities are calculated from their energies relativistically, so the velocity distribution is highly dependent

8

on the energy distribution. This section presents the theory and modelling of the electron energy distribution from an arbitrary neutron spectrum.

The free neutron beta decay spectrum has been investigated for many years, but until recently the equipment required to observe the electron spectrum from free neutrons near rest has not been available. Golub, et al., proposed research in this field by using cryogenic bottles to contain free neutrons for observation (Ref 10:134). Unfortunately, this data has not been published yet, and could not be used in this study. However, the neutron beta decay spectrum measured in 1951 by Robson is reliable and is still being used today (Ref 9:352, 11:378). It was thus chosen for this study.

Figure 1 shows Robson's thermal neutron decay beta spectrum with his curve fit for the data. Since no information was available on the
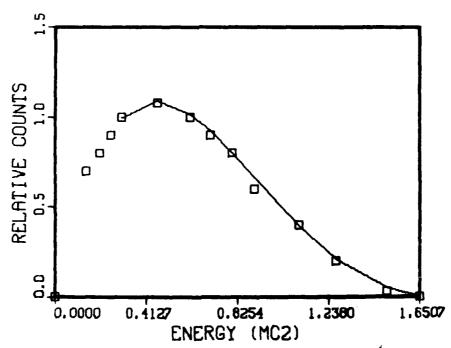
Fig. 1 The Experimentally Observed Neutron
Beta Decay Energy Spectrum

9

lower energy electrons, this author speculated the zero energy

intercept and used the .4 $m_o c^2$ (m_o is the electron rest mass) and

higher energy data points to generate coefficients for a polynomial

curve fit. A fourth order polynomial fit was shown to fit the data

with a Chi-square value of .2521, which is off by less than 0.5

percent. The unnormalized polynomial fit is shown in equation 2

with electron energy (in $m_o c^2$) as the independent variable.

$$P(E) = .0268061907 + 5.554304753E - 9.207097299E^2 + 5.101880231E^3 - .9502414486E^4 \tag{2}$$

Figure 2 shows the superposition of this curve fit normalized

with the experimental data. Robson's data shows the maximum electron

energy at 844 keV. Theoretically, the maximum electron energy

should be 785 keV. The higher value is within experimental error
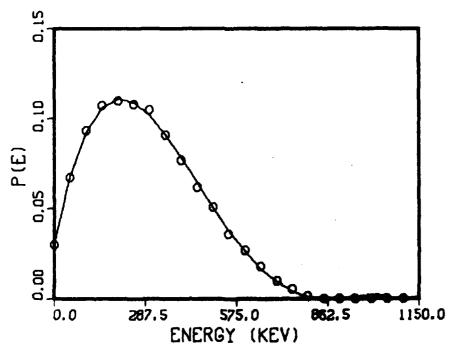
Fig. 2   Beta Energy Spectrum from Neutron Decay
Curve Fit Superimposed Over Data

of the theoretical limit, and, not knowing the nature of the error, the errors caused by forcing the data to fit the theoretical limit would be unpredictable and possibly invalidate the entire spectrum. Therefore, the higher energy electrons were included in the model.

This beta spectrum will depend on the neutron energy. Assuming that the electron and proton, decay products, possess the same velocity as the neutron before it decays, the neutron velocity must be added relativistically to the velocity each particle obtains from the decay energy. Since we are considering relativistic particles, velocity addition dramatically increases the electron energy in order to conserve momentum. Hence, increasing neutron energy skews and squashes the electron energy spectrum. Figure 3 shows the difference between the beta spectra of 0 and 19.64 MeV neutrons. These two curves represent the two extremes expected for neutron energies from bomb neutrons.

Fourth order polynomial curve fits were calculated for each neutron energy group, and then each fit constant was found as a function of neutron energy. The general equation determining the electron spectra from an arbitrary neutron spectrum is shown in equation 3. Appendix B presents the polynomial fit constants of the beta spectrum curve fits

$$N(E_n, E_e) = b_0(E_n) + b_1(E_n)E_e + b_2(E_n)E_e^2 + b_3(E_n)E_e^3 +$$

$$b_4(E_n)E_e^4 \qquad\qquad (3)$$
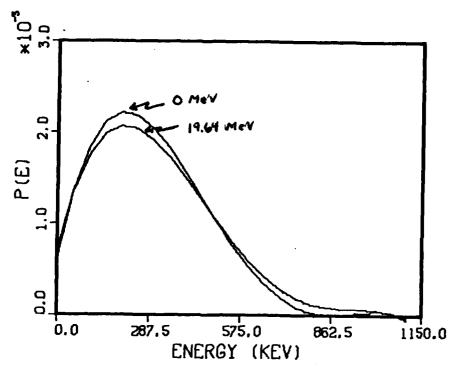
Fig. 3 Normalized Beta Energy Spectra for
0 MeV and 19.64 MeV Neutrons

for various neutron energies. The neutron energy groups were chosen

to coincide with the important neutron energy groups for calculating

the neutron induced secondary gammas since they were already used in

the PROMPT code (Ref 12:7).

The curves fitting the fit constants for arbitrary neutron

energies is also given in Appendix B. These constants correspond to

the b_n in equation 3. Since the neutron energy groups are narrow,

linear interpolation between the fit constants could be used as a

convenient way to calculate the coefficients. Equation 3, however,

provides slightly more accurate results with less computer space.

An example compares the expected curve fit found with equation 3 to

the linear interpolation between the 12.82 MeV and the 13.84 MeV

neutron energy groups. A neutron energy of 13.00 MeV is used for

12

comparison. To determine the error, another monte-carlo run was made for this neutron energy. The difference between the equation 3 result and the monte-carlo result is .08%, while the difference was .12% for linear interpolation.

Since the equations are normalized, the electron spectrum from any type of neutron spectrum can now be found. Arbitrary electron energy groups can be defined to acquire information on the electron spectrum from bomb neutron decay. These groups are defined between the energies E_i and E_{i+1}. Integrating equation 2 determines the expected number of electrons per source neutron between the energies E_i and E_{i+1}. This result can be multiplied by the number of neutrons that decay in that neutron energy group and then summed over all neutron groups. Equation 4 summarizes this calculation.

$$N_{e_{E_i}} = \sum_{j=0}^{m} N_{n_{E_j}} \sum_{\ell=0}^{4} \frac{a_\ell(E_j)(E_{e_{i+1}} - E_{e_i})^{\ell+1}}{(\ell+1)} \qquad (4)$$

In equation 4, $N_{e_{E_i}}$ is the number of electrons with energy between E_i and E_{i+1}. $N_{n_{E_j}}$ is the number of neutrons with energy E_j of the j th neutron energy group that decay, and a_ℓ are the appropriate polynomial curve fit coefficients found in Table B-I of Appendix B.

Electron Angular Distribution from Neutron Decay

In addition to the electron energy distribution, the electron angular distribution must be known to model the trapped electron distribution. This section presents the theory and modelling of the electron angular distribution from neutron decay.

Theoretically, the electron energy limit imposed by the decay energy is 785 keV. Any electron observed at a higher energy must originate from an energetic neutron. The fastest electron possible from a decay must be scattered forward at zero degrees from the neutron velocity vector. The slowest electron will be one emitted opposite to the neutron velocity vector. This indicates that the electron angular distribution depends on both the electron energy and the neutron energy.

The final electron energy distribution from the decay is different for different neutron energies. This correlation was derived in equations 2 and 3. Each spectrum is different because the neutron adds velocity to the electron and tends to skew the electron angular distribution forward, as shown in figure 4. However, the *electron angular distribution* also depends on the electron
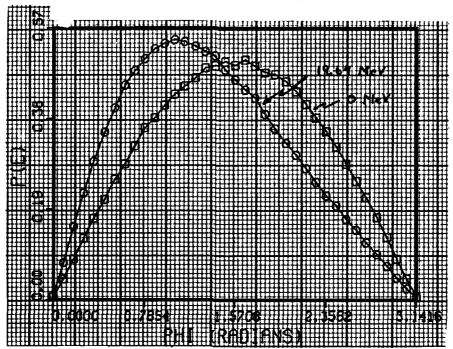
Fig. 4 Angular Distribution of Electrons from
a 0 MeV and a 19.64 MeV Neutron

14

energy distribution because a 14 MeV neutron can create a 1 MeV electron. However, to conserve momentum and energy, the 1 MeV electron will only be observed at an angle very forward scattered. Modelling this information independent of electron energy might be useful to observe the scatter distribution of the electrons as figure 4 shows. But, the important information is the relationship between electron energy and its angular distribution. This relationship depends on both the electron and the neutron velocities. Appendix C shows the angular distribution of 0-50 and 500-550 keV electrons for various neutron energies. It assumes isotropic decay in the center of mass reference frame.

Assuming that the decay of neutrons at rest is isotropic, the same general monte-carlo method that generated the energy spectra simultaneously generated the angular information. Simultaneous generation is critical since the electron angular distribution greatly influences the electron energy distribution for a specific neutron energy as found in the previous section. The electron angular distribution depends on neutron energy and electron energy. However, figure 4 shows the angular distribution for all electrons, independent of electron energy, per source neutron of a zero and a 19.64 MeV neutron.

For electrons originating from 0 to 19.64 MeV neutrons, the electron spectrum ranges from 0 to 1.1 MeV. This electron energy range was broken into 50 keV energy groups for angular distribution modelling. Fourth order curve fits were found for each 50 keV group for 12 neutron energies to solve equation 5, where θ is in radians.

15

$$P(\theta) = a_0(E_n) + a_1(E_n)\theta + a_2(E_n)\theta^2 + a_3(E_n)\theta^3 + a_4(E_n)\theta^4 \qquad (5)$$

This data base was very large, so a 7th order curve fit for each a_i dependent on neutron energy was found. Equation 6 is used to calculate the a_i using the fit constants presented in subroutine ANGLE of Appendix E.

$$a_i(E_n) = b_0 + b_1 E_n + b_2 E_n^2 + b_3 E_n^3 + b_4 E_n^4 + b_5 E_n^5 + b_6 E_n^6 +$$

$$b_7 E_n^7 \qquad (6)$$

where the E_n are in keV.

From this data base, the distribution of electron angles for electrons in specific 50 keV groups can be found. The a_i fit coefficients for a specific 50 keV energy group can be found for each neutron energy group. These coefficients are used to calculate the electron angular distribution by integrating equation 5 and defining angular bins to any specified detail.

Since the electron's angle with the magnetic field line is important to calculate the particle motion, a correlation between the decay angle and the magnetic field line is required. Appendix D derives the relation between a neutron incident on a magnetic field line and the electron density as a function of an angle α from the magnetic field line. The procedure outlined in Appendix D can be used to numerically evaluate the number of electrons between α and $\alpha + d\alpha$ from a field line. This technique requires transforming

the coordinates of equation 5 into coordinates defined around the magnetic field line.

Chapter IV

Distribution Modelling

The Air Force Weapons Laboratory computer code PROMPT calculates neutron, gamma, and x-ray spectra from nuclear detonations for points in space from the prompt radiation. Since electrons create hazards in space, the capability to calculate the electron spectrum and flux at a point in space from neutron decay needed to be added. This chapter is devoted to how the theory developed in the previous chapters was added to PROMPT. The subroutines are provided in Appendix E with a user's manual.

Electron Energy Spectrum

The electron energy spectrum developed early in Chapter III depends on the bomb neutron energy spectrum. Since the PROMPT code already calculates the neutron spectrum at a point, this information provides the electron density and the electron energy distribution from each neutron energy group. Taking the electron spectrum curve fit constants as determined by the neutron energy applied to the constants of Table B-II in Appendix B, the electron energy spectrum for each of the 38 neutron energy groups is found. Using 50 keV electron energy groups for spectral shaping, 23 electron groups between 0 and 1.15 MeV contain the electron density distribution from neutron decay.

Applying equation 1 to the neutron density, and taking into account the time dilation of the half life of the higher energy neutrons, the electron density from neutron decay is found. This calculation uses the lower neutron energy from each neutron energy group. Taking each neutron energy group separately, the electron energy spectrum is integrated and the number of electrons in each 50 keV electron energy group is found by multiplying the number of decayed neutrons by the expected number of electrons in each electron energy group per source neutron. The total number of electrons in each of these energy groups is found by summing the contributions from all neutron energy groups. The resulting distribution is the desired total electron energy spectrum.

Electron Angular Distribution

The electron angular distribution developed in the later part of Chapter III shows that the angular distribution depends on both the neutron and the electron energies. For a point in space, this subroutine was developed to calculate the angular distribution with respect to the forward scattered angle of θ radians. The method to calculate this distribution begins by calculating the curve fit coefficients, the a_i in equation 7, of the electron angular distribution for each neutron energy group. Equation 7 requires the neutron group energy E_n and the polynomial fit coefficients b_{ji} of the ith electron energy group. The resulting angular distribution of electrons decaying from a specific energy neutron are modelled with fourth order curve fits. For a specific electron energy, this distribution determines the $N_{E_e}(\theta)$ in equation 8. This distribution

is applied to each of the electron energy groups previously mentioned, except that this distribution depends on the 0-50, 50-100,.., 1100-1150 keV electron energy groups specifically because the curve fit constants were derived dependent on these groups.

$$a_i(E_n) = \sum_{j=0}^{7} b_{ji} E_n^{j} \tag{7}$$

$$N_{E_{e,n}}(\theta) = \sum_{i=0}^{4} a_{in} \theta^{i} \tag{8}$$

Each of these fourth order equations are integrated to determine the distribution of electrons between specific angular groups. The total number of electrons are then multiplied by the angular distribution function for electrons just determined. This method is repeated for each neutron energy group until all the electrons from each neutron group are distributed into the angular bins. Equation 9 presents the calculation of the total angular distribution of electrons with respect to the angle from the forward neutron velocity. $N(\theta)$ is the distribution of electrons at an angle θ, N_e is the total number of electrons, E_{n_i} is the neutron energy of the ith group, and the other parameters are consistent with equations 7 and 8.

$$N(\theta) = N_e \sum_{i=1}^{37} \sum_{j=0}^{4} \left[\left(\sum_{k=0}^{7} b_k E_{n_i}^{k} \right) \theta^{j} \right] \tag{9}$$

The angular information is important to determine the electron life span in the magnetosphere. Since the flux depends on electron energy, by virtue of the velocity, the flux will vary with time as

20

the electrons leave the trapped region. Therefore, the angular

distribution of electrons with specific energies relative to the

magnetic field must be known. Because of this problem, as well as

the problem that the angular distribution depends on both the elec-

tron and neutron energy, the total angular distribution is of little

applicable use, but the subset of distributions are critical for

flux, time dependent models. Appendix E addresses the numerical

solution to this part of the problem.

One should note that PROMPT provides the neutron spectra at a

point in space, but it does not provide any information concerning

the angular nature of the neutrons. Due to scatter in the atmosphere,

some neutrons may not arrive radially from the burst. In a homoge-

neous atmosphere, however, one would expect the average neutron to

arrive radially from the burst. This means that the results of this

study would hold true in an average sense. An inhomogeneous atmos-

phere would be impossible to handle with PROMPT because the neutron

angular distributions require significantly more sophisticated

techniques. Assuming radial neutrons serves as a source of error in

the electron angular distributions, but, given the correct neutron

angular information, the theory and method could be simply extended.

Chapter V

Flux Calculations in the Magnetosphere

Foundations

Since the discovery of trapped radiation in the magnetosphere, many people have wondered about the underlying physical properties involved in this phenomenon. Experiments designed to study particle motions in the magnetosphere used charged particle accelerators as well as nuclear weapons to inject large numbers of charged particles into the magnetosphere. Probably the world's most noted experiment of this sort, Starfish, injected numerous charged particles that became trapped in the magnetosphere for years.

Modelling the injection process for bursts like Starfish begins with magnetohydrodynamic calculations of the plasma interaction with the magnetic field. From this interaction, the fission debris distribution is found, and electron injection from this debris is calculated. Electrons move between mirror points and drift around the earth, forming electron belts. Some belts are more stable than others because decay processes like atmospheric absorption, collisions, plasma instabilities, and many other complicated mechanisms, decrease the electron density in these belts with time (Ref 2).

The purpose here, is to calculate prompt electron fluxes from neutron decay electrons injected into the atmosphere or magnetosphere. The source of decaying neutrons is prompt neutrons from the fission

and fusion processes. Instead of plasma interactions, particle transport methods propagate the neutrons through real atmosphere to find the neutron spectrum at a point in space.

The neutron transport method for this investigation uses mass integral scaling fits of two dimensional anisotropic neutron transport S_n solutions. These equations are part of the PROMPT computer code owned and maintained by the Air Force Weapons Laboratory at Kirtland Air Force Base in New Mexico. For medium to high altitude bursts, the neutron transport calculations are in error by less than a factor of two (Ref 13). PROMPT calculates neutron, gamma, and x-ray spectra at a point in space. The additional capability to calculate electron spectra from the decaying neutrons was added during this study to round out the code capabilities.

Electron Flux Parameters

Electron flux depends on the number of electrons passing through a region of space per unit time. The essential information for flux calculations can be found in the electron spectrum and the electron density. However, in the magnetosphere, the electron interaction with the magnetic field tends to reduce the electron density with time and to change the spectrum. For the purpose of this paper, the object is to calculate the prompt electron flux. Time dependencies were not calculated since only the source was being investigated.

Techniques have been published to calculate fluxes along field lines, (Ref 14) but the electron spectrum and density must be known for each point along the field line. Since the foundation of the prompt calculation is the mass integral, a relation between the mass

23

integral and the electron flux was found. The flux is directly proportional to the number of neutrons, and if one assumes the spectrum does not change with yield, the relation between flux and yield is linear.

Using the PROMPT code with an unclassified thermonuclear spectrum, the electron fluxes as a function of mass integral for 1 kiloton bursts were calculated and are presented in Table I. The method used to calculate the values in Table I first chose a 1 kt burst at the altitude in the left column. The electron flux was then calculated at a point 400 km above the burst point. PROMPT calculated the mass integral in column two and the DECAY subroutine, developed in this study, calculated the fluxes in column three. Figure 5 plots the electron flux dependence on mass integral from Table I.

Table I

Electron Flux as a Function of Mass Integral

Burst Altitude km	Mass Integral gm/cm^2	Electron Flux e^-/cm^2-sec
2	8.201E+02	3.935E-09
5	5.530E+02	1.366E-04
10	2.686E+02	1.025E+01
12	1.978E+02	1.957E+02
15	1.237E+02	4.392E+03
20	5.590E+01	5.502E+04
25	2.556E+01	1.117E+05
27	1.885E+01	1.171E+05
30	1.208E+01	1.124E+05
40	3.049E+00	7.989E+04
50	8.584E-01	6.721E+04
60	2.380E-01	6.536E+04
75	2.652E-02	6.703E+04
100	3.598E-04	6.703E+04
--	0.0	5.823E+04

Table I shows that the flux does not necessarily monotonically increase as the mass integral decreases. As the burst altitude increases, the mass integral decreases, but the neutrons have a greater tendency to reflect off the denser lower atmosphere. This phenomenon is a combination of albedo and build up and is caused by neutron scatter in the atmosphere. The scattered neutrons increase the neutron, and, thus, the electron density or flux. This albedo effect has its highest influence below 40 km. Outside this range, the albedo neutrons are either not produced or are negligible because of spherical divergence. With no atmosphere, 0 gm/cm^2, no build up or albedo is observed. Hence, the last flux value in Table I is less than the other values.

Comparing the fluxes of Table I to the expected fluxes calculated for a vacuum in Appendix A, Table I fluxes are higher than Appendix A fluxes until the mass integral goes over 100 gm/cm^2. The discrepancy here lies in the albedo neutrons, which increase the electron density, and a higher average electron energy than that used in Appendix A. These two factors combined are enough to increase the observed flux by the appropriate amount because albedo alone can increase the neutron density by a factor of 2 or more depending on the mass integral.

Another way to examine the mass integral effect on electron flux is to take an observer at a constant altitude and change the height of the burst directly below it. For this example a 500 km observer was chosen. The burst was 1 kt directly below the target at various altitudes. Table II presents the mass integral in gm/cm^2 and the electron flux in electrons/cm^2-sec for each burst altitude.

The information presented in Table II is useful to show the general tendency that very low altitude bursts make little

25
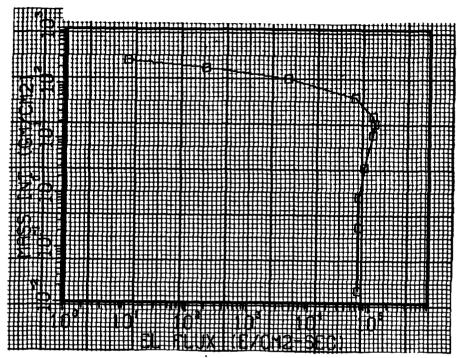
Fig. 5 Electron Flux Dependence on Mass Integral
for a Constant 400 km Distance

Table II

Electron Flux as a Function of Mass Integral
for a 500 km Observer

Burst Altitude km	Mass Integral gm/cm^2	Electron Flux e$^-$/cm^2-sec
2	8.201E+02	2.539E-09
5	5.530E+02	8.920E-05
10	2.686E+02	6.832E+00
12	1.978E+02	1.315E+02
15	1.237E+02	2.987E+03
20	5.590E+01	3.821E+04
25	2.556E+01	7.919E+04
27	1.885E+01	8.375E+04
30	1.208E+01	8.140E+04
40	3.049E+00	6.041E+04
50	8.584E-01	5.311E+04
60	2.380E-01	5.402E+04
75	2.652E-02	5.938E+04
100	3.598E-04	6.703E+04

contribution to the electron environment from neutron decay. However, it also shows that bursts have increasing effect on the electron environment up to about 30 km due to albedo and build up. Bursts above 30 km have decreasing effect as the albedo and build up factors have smaller influence since the mass integral decreases. When the mass integral becomes small enough that neutron attenuation is negligible, between 50-60 km, the electron flux increases since more neutrons reach the target. A plot of mass integral influence on the flux observed at a 500 km target is shown in figure 6.

Fig. 6 Electron Flux Observed at a 500 km Observer
Over a 1 kt Burst at Different Altitudes

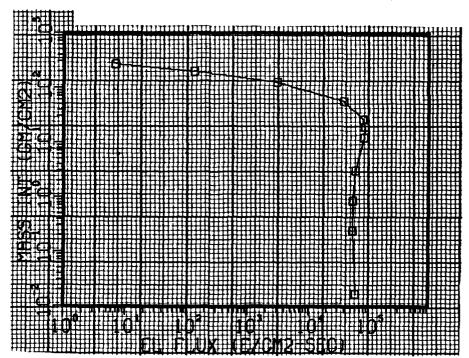One other parameter essential for magnetospheric flux calculations is the electron angular distribution with respect to the magnetic field line. Electron density in the magnetosphere decays with time as the electrons trapped in the magnetic field interact

with other particles and fields. The loss cone is one of the more important loss mechanisms for the newly formed electron belts. The loss cone can be defined as the minimum angle at which electrons can intersect the magnetic field line and mirror. Electrons with angles less than the loss cone angle will not be trapped. Instead, they are absorbed by the atmosphere. This loss mechanism rapidly decreases the electron density along a field line and decreases the observed electron flux. Although calculating the actual flux after the electrons have dispersed along the field line is beyond the scope of this thesis, the angular distribution of the electrons with respect to the field line is calculated and the underlying method is presented in Appendix E.

Each of these parameters show why the observed flux should be lower than the calculated flux soon after the prompt radiation is created. The electron density is greatly dependent on slant range due to divergence and neutron attenuation. Other places along a magnetic field line could be considerably closer to the burst than where the satellite must pass the field line. These considerations show that the prompt interaction with the entire field line must be calculated to determine the true electron density in the region that the satellite passes. However, when the satellite observes the prompt radiation, the electron flux from the prompt neutrons should be observed as the theory predicts.

Validation of the Theory

Because data on prompt radiation observations are unavailable, checking theory with observation is not possible. However, early

time information was available from the Teak event when Explorer IV reported fluxes of 10^4 (e^-/cm^2-sec) for electron energies greater than 580 keV 18 minutes after the burst.

These fluxes were reported when the satellite was over Singapore. Unfortunately, the position of the satellite is not well-known. Some references indicate that Explorer IV was between 1400 and 1600 kilometers in altitude at 99°E. The Teak event occurred at 17°N 191°E and an altitude of 80 km. The satellite could not observe any prompt radiation because it was below the horizon. The magnetic field lines near the satellite never came above the horizon either (Ref 15). Thus, the electron fluxes observed by Explorer IV must remain an open question.

No other early time information was available for any other burst, so observational support of the results of this study does not exist. Unless more accurate information on the position of Explorer IV, 18 minutes after Teak, becomes available no verification can be made. The fluxes of 3×10^4 e^-/cm^2-sec could be observed a maximum of 4×10^4 km from the burst.

Chapter VI

Conclusions and Recommendations

The purpose of this research was to model the neutron decay influence on the electron space environment. During this investigation, the neutron decay phenomenon was broken into the resulting electron energy and angular distribution as a function of neutron energy. Assuming that the decay is isotropic in the center of mass frame and that the neutron velocity added to the product velocities from the decay process, it was found that the neutron energy greatly influenced both the electron energy and the angular distributions. By theory, the electron energy limit is only 785 keV, but, by adding the neutron velocity relativistically, electron energies above 1.1 MeV could be observed. These higher energy electrons were forward scattered as were the rest of the electrons from the higher energy neutrons. The existence of the higher energy electrons added greatly to the expected fluxes. The actual damage these electrons cause depends on the materials and the shielding they interact with, however, fluxes greater than what one would expect from spherical divergence in free space were calculated because of neutron scatter off the earth's denser atmosphere. The resulting fluxes were higher than normal background radiation in the electron belts and, when fission debris is not a major source of electrons, neutron decay can serve as a significant source by itself.

By determining that the flux observed 400 km from a 1 kt burst yields fluxes near 10^5 electrons/cm^2-sec, and that the flux is directly proportional to yield, any burst above 20 km becomes a significant source of electrons hundreds of kilometers from the burst point. Even for a constant altitude observer at 500 km, varying the burst altitude showed a maximum electron flux near 30 km. The albedo and build up factors cause the different fluxes due to the amount of neutrons they scatter towards the observer. Since the electron flux is directly proportional to the number of neutrons, for a detonation with a similar neutron spectrum, the electron flux increases linearly with yield. Cases were looked at to explain the Explorer IV data, but uncertainty in the position of the satellite precluded any sound verification of the theory. No other observational evidence was available to compare with results of this study.

The most probable regions of errors would be in the transport and the decay spectra. Due to the significant influence of the neutron spectrum on the resulting electron flux, the largest source of error would be the neutron transport calculation. The error in the neutron spectrum for bursts above 20 km is less than a factor of two, while lower altitude bursts can generate errors up to one order of magnitude. The major assumption underlying the theory of neutron decay was the isotropic decay scheme. If the neutron does not decay isotropically, the electron energy and angular spectra would both be modelled incorrectly. The error caused by this assumption is probably negligible.

This thesis used purely analytical methods to model the electron spectra as functions of neutron energy. The probability distributions were complicated functions, yet the energy distribution was observed to be similar to a Planckian distribution that flattened and skewed with increasing neutron energy. Using the neutron energy as a temperature may simplify the modelling process and improve its accuracy. Presently, the only data available on the electron spectrum comes from a 1951 experiment. Theories do not exist to explain the low energy electron spectrum and could be investigated using a Planckian distribution scheme.

Until more information is available from satellite data, including satellite positions, and from theoretical development of the distribution functions, no validations can be made to improve this procedure. Better approximations of the electron fluxes from neutron decay can be made by improving the transport calculations, the spectral information, or even the curve fit solutions, but the expected error is less than a factor of 4. The necessary information to provide an accurate validation of this theory is accurate early time satellite data of a high altitude nuclear detonation.

The general conclusions of this study are:

1. the electron energy distribution in the lab frame is greatly affected by the neutron energy.
2. the electron angular distribution in the lab frame depends on the electron energy as well as the original neutron energy.
3. the electron energies from neutron decay are generally in the region influencing satellite charging phenomena.
4. the electron flux from this source can be significantly higher than background.

With more research, the complete impact of this source on satellite survivability/vulnerability can be found. The areas that need to be investigated further are:

1. accurate satellite data including satellite position of early time electron flux observations of any high altitude test,
2. investigate using the Planckian distribution to model the electron energy spectrum from neutron decay,
3. investigate the impact of this source over an entire magnetic field line, and
4. incorporate the effect of an incident neutron angular distribution on the magnetic field line flux.

Once these areas have been studied, a complete analysis of the problem should be realized.

Bibliography

1. Backstrom, Robert C., _Anomalous Transport Coefficients Due to the Ion-Ion Two Stream Instability_, Dissertation. Wright-Patterson AFB, Ohio: School of Engineering, Air Force Institute of Technology, 1978.

2. Foster, D. F., et al., _Experimental Series Parameters for the Decay of Multigroup Beta and Gamma Spectra from .1 to 1000 Seconds After a Fission Burst_, AFWL-TR-78-4 (November, 1978).

3. Hess, Wilmot N., _The Radiation Belt and Magnetosphere_, Toronto: Blaisdell Pub. Co., 1968.

4. Killeen, John, et al., "Electrons from Bomb Neutron Decay," _Journal of Geophysical Research_, _Vol. 68_ (No. 16): 4637-4643 (August 15, 1963).

5. DASA Report #2309, _Review of Artifical Radiation Belts, Explorer 4; Unidirectional Trapped Radiation, Injun 1_, St. Louis University Physics Dept., St. Louis, Mo. 1969.

6. General Electric, _Chart of the Nuclides_, 1972.

7. Singley, G. W., _A Model Environment for Outer Zone Electrons_, NSSDC 72-13; National Space Science Data Center, December 1972.

8. Cladis, J. B., et al., (editors), _The Trapped Radiation Handbook_, DNA 2524H; Defense Nuclear Agency, January 21, 1977.

9. Robson, J. M., "The Radioactive Decay of the Neutron," _Physical Review_, _Vol. 83_ (No. 2): 349-358 (July 15, 1951).

10. Golub, et al., "Ultracold Neutrons," _Scientific American_: 134-154 (June, 1979).

11. Erdzolimskii, B. G., "Beta Decay of the Neutron," _Uspekhi_, _Vol. 18_: 377-386 (May 1975).

12. Murphy, Harry M., _PROMPT II, A Module to Calculate Neutron, Gamma, and X-Ray Spectra from a Near Exoatmospheric Nuclear Detonation_, AFWL-NTY-TN-81-1, 26 January 1981.

13. AFWL-TR-76-142, _High Altitude Atmospheric Radiation Transport Calculations_, Kaman Sciences Corp., August, 1976.

14. Hess, W. N., Killeen, J., "Spatial Distribution of Electrons from Neutron Decay in the Outer Radiation Belts," *Journal of Geophysical Research*, *Vol. 66* (No. 11): 3671-3680 (November, 1961).

15. Greaves, Captain Robert J., Satellite and C^3 Branch, Air Force Weapons Laboratory, Kirtland AFB, New Mexico, June 1980 - December 1981, Private Communications.

Appendix A

Electron Flux from Decaying Neutrons

This appendix addresses an ideal calculation of the number of neutrons decaying at a point in space and the electron flux at that point. Assuming no attenuation of the neutrons from the burst and no build up factor or albedo factor, the neutron density that decays satisfies the equation,

$$N = \frac{S}{4\pi R^2 v_n \tau} \qquad \text{(A-1)}$$

where N is the number of neutrons per unit volume a distance R from a burst that decay, S is the initial number of source neutrons, v_n is the neutron velocity, and τ is the neutron mean lifetime. Additionally, all neutrons are assumed to have the same energy.

For a 1 kiloton bomb, approximately 10^{23} neutrons are released with a mean energy of 1.2 MeV. This energy corresponds to an average neutron velocity of 1.51×10^9 cm/sec. Since the neutron half life is 10.6 minutes (Ref 6), τ is 919 seconds.

To determine the electron flux, equation A-1 must be multiplied by the electron velocity. Using an average electron energy of 600 keV, the average electron velocity is 2.66×10^{10} cm/sec. Table A-I tabulates the expected electron flux as a function of distance from a 1 kt burst. The fluxes calculated for Table A-I

Table A-I

Neutron Density and Electron Flux
from a 1 kt burst

R(km)	N (e$^-$/cm^3)	Flux (e$^-$/cm^2-sec)
.1	5.718E+01	1.523E+12
1.	5.718E-01	1.523E+10
10.	5.718E-03	1.523E+08
100.	5.718E-05	1.523E+06
1000.	5.718E-07	1.523E+04
10000.	5.718E-09	1.523E+02

are highly spectral dependent. Therefore, the accuracy is limited

because of the error from assuming all neutrons have the same energy.

Since the mean electron energy from neutron decay is a little below

600 keV, using 600 keV as an average energy keeps the error within

an order of magnitude. Therefore, these estimates can be used to

approximate the general flux one might expect from this situation.

Appendix B

Decay Electron Energy Spectra Curve Fitting

This section presents fit coefficients for the electron energy spectrum. Least squares polynomial curve fits with equal weighting of all data points established the equations discussed in this section. Table B-I lists the fourth order fit coefficients to the equation:

$$P(E_e) = a_0 + a_1 E_e + a_2 E_e^2 + a_3 E_e^3 + a_4 E_e^4 \qquad (B-1)$$

where E_e is the electron energy in keV. $P(E_e)$ is the probability of observing that energy electron and the a_i are the fit coefficients dependent on neutron energy. Table B-II presents the second order fit coefficients to the a_i in the above equation. These coefficients, labeled b_n, satisfy the equation:

$$a_i(E_n) = b_{0_i} + b_{1_i} E_n + b_{2_i} E_n^2 \qquad (B-2)$$

where E_n is the neutron energy in keV between 0 and 1.964E+04 keV.

Special attention must be made when using these fits. They are only good for interpolating between 0 and 19.64 MeV. Care must be taken to ensure that the energy bounds in both equations are not exceeded.

Appendix B

Table B-I

Polynomial Fit Constants of the Electron Spectrum for Different Neutron Energies

E_n (MeV)	a_0	a_1	a_2	a_3	a_4
1.964E+04	7.188E-04	1.525E-05	-5.294E-08	5.779E-11	-2.076E-14
1.691E+04	7.092E-04	1.540E-05	-5.342E-08	5.822E-11	-2.086E-14
1.492E+04	7.028E-04	1.562E-05	-5.420E-08	5.908E-11	-2.117E-14
1.419E+04	6.995E-04	1.571E-05	-5.450E-08	5.941E-11	-2.128E-14
1.384E+04	6.995E-04	1.573E-05	-5.458E-08	5.949E-11	-2.130E-14
1.282E+04	6.925E-04	1.589E-05	-5.508E-08	6.002E-11	-2.149E-14
1.221E+04	6.876E-04	1.600E-05	-5.546E-08	6.047E-11	-2.165E-14
1.105E+04	6.842E-04	1.612E-05	-5.589E-08	6.093E-11	-2.181E-14
1.000E+04	6.811E-04	1.624E-05	-5.634E-08	6.147E-11	-2.201E-14
9.048E+03	6.747E-04	1.639E-05	-5.683E-08	6.200E-11	-2.220E-14
8.187E+03	6.725E-04	1.649E-05	-5.719E-08	6.241E-11	-2.234E-14
7.408E+03	6.715E-04	1.655E-05	-5.742E-08	6.264E-11	-2.242E-14
6.376E+03	6.550E-04	1.668E-05	-5.779E-08	6.299E-11	-2.251E-14
4.966E+03	6.630E-04	1.683E-05	-5.835E-08	6.364E-11	-2.275E-14
4.724E+03	6.603E-04	1.688E-05	-5.853E-08	6.384E-11	-2.282E-14
4.066E+03	6.532E-04	1.704E-05	-5.911E-08	6.453E-11	-2.309E-14
3.012E+03	6.493E-04	1.715E-05	-5.945E-08	6.488E-11	-2.320E-14
2.385E+03	6.424E-04	1.730E-05	-5.997E-08	6.549E-11	-2.343E-14
2.307E+03	6.426E-04	1.729E-05	-5.994E-08	6.543E-11	-2.340E-14
1.827E+03	6.428E-04	1.732E-05	-6.003E-08	6.552E-11	-2.342E-14
1.108E+03	6.314E-04	1.753E-05	-6.072E-08	6.631E-11	-2.372E-14
5.502E+02	6.239E-04	1.769E-05	-6.131E-08	6.703E-11	-2.400E-14
1.576E+02	6.137E-04	1.788E-05	-6.199E-08	6.787E-11	-2.434E-14
1.111E+02	6.096E-04	1.796E-05	-6.228E-08	6.823E-11	-2.449E-14
5.248E+02	6.083E-04	1.799E-05	-6.246E-08	6.849E-11	-2.461E-14
2.479E+02	6.077E-04	1.802E-05	-6.258E-08	6.867E-11	-2.469E-14
2.188E+01	6.079E-04	1.802E-05	-6.257E-08	6.866E-11	-2.468E-14
1.033E+01	6.073E-04	1.802E-05	-6.257E-08	6.864E-11	-2.467E-14
3.355E+00	6.055E-04	1.805E-05	-6.268E-08	6.879E-11	-2.473E-14
1.234E+00	6.051E-04	1.807E-05	-6.275E-08	6.889E-11	-2.478E-14
5.830E-01	6.052E-04	1.806E-05	-6.273E-08	6.885E-11	-2.476E-14
1.013E-01	6.051E-04	1.807E-05	-6.274E-08	6.887E-11	-2.477E-14
2.902E-02	6.048E-04	1.807E-05	-6.276E-08	6.889E-11	-2.478E-14
1.068E-02	6.048E-04	1.807E-05	-6.276E-08	6.889E-11	-2.478E-14
3.059E-03	6.050E-04	1.807E-05	-6.276E-08	6.890E-11	-2.478E-14
1.125E-03	6.051E-04	1.807E-05	-6.276E-08	6.890E-11	-2.478E-14
4.140E-04	6.051E-04	1.807E-05	-6.275E-08	6.889E-11	-2.478E-14
1.000E-08	6.050E-04	1.807E-05	-6.276E-08	6.890E-11	-2.478E-14

Appendix B

Table B-II

Fit Constants for Electron Energy Spectra
from Arbitrary Neutron Energies

$b_n(E_n(kev))$	b_0	b_1	b_2
b_0	6.093E-04	1.076E-08	-3.036E-13
b_1	1.799E-05	-2.364E-10	5.214E-15
b_2	-6.244E-08	8.373E-13	-1.903E-17
b_3	6.847E-11	-9.915E-16	2.415E-20
b_4	-2.460E-14	3.797E-19	-9.962E-24

Appendix C

Electron Angular Distribution Dependence
on Electron and Neutron Energies

To show the dependence of the electron angular distribution on
both the electron and neutron energies, this appendix presents a
series of plots. The data for each plot are the results of the
monte-carlo simulation described in Chapter III. Each plot presents
the 0-50 keV electron energy group-□ and the 500-550 keV electron
energy group group-0 for twelve neutron energy groups. The scales
are linear on both axes and present the probability of observing an
electron created by the appropriate neutron of a specific energy as
a function of angle. The angle is defined in radians from 0-π where
a 0 angle indicates scatter in the direction of the neutron velocity
vector and a π angle indicates backscatter against the neutron
velocity vector.

Isotropic decay in the center of mass reference frame was
assumed, so the low energy neutrons should, and do, produce such an
isotropic distribution. The higher energy neutrons should skew the
faster electrons more forward, while the slower electrons remain
nearly isotropic.

The reason for this co-dependence is that the resulting electron
angular distribution depends on the velocity addition of the neutron
and the electron velocities. Since the center of mass energy
distribution remains constant and the center of mass decays

41

isotropically, the lab frame will observe skewed angular distributions that peak in the direction forward to the perpendicular of the neutron velocity. The energy spectrum in the lab frame will also be skewed to higher energies and change the energy distribution. Since the expected number of electrons of a specific lab frame energy change, so will the overall distribution of the angles those electrons will be seen. Figures C-1 through C-12 show the numerical support from the monte-carlo simulation.

Comparing the angular distributions of all electron energy groups caused by a specific neutron energy with each other, it is obvious that the angular distributions are different except for those distributions from the very low energy neutrons. Looking at the angular distribution of a specific electron energy group as the neutron energy changes, it is observed that this distribution also changes. The higher energy electrons are skewed more forward with increasing electron energy, while the lower energy electron angular distributions are squashed, but remains fairly isotropic. These observations indicate that the electron angular distribution from neutron decay depends on both the electron and the neutron energy.
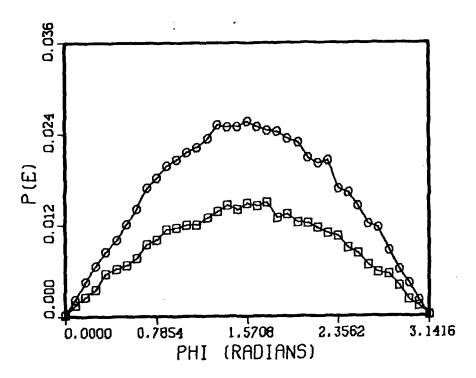
Fig. C-1   0-50 and 500-550 keV Electron Group Angular
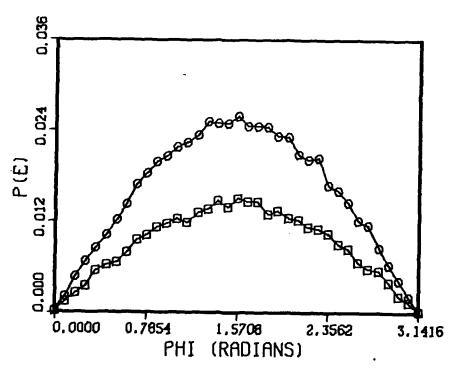Distributions from 1.125E-03 keV Neutron

Fig. C-2   0-50 and 500-550 keV Electron Group Angular
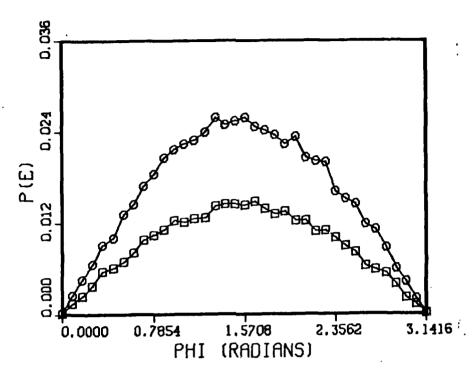Distributions from 5.830E-01 keV Neutron

43

Fig. C-3 0-50 and 500-550 keV Electron Group Angular
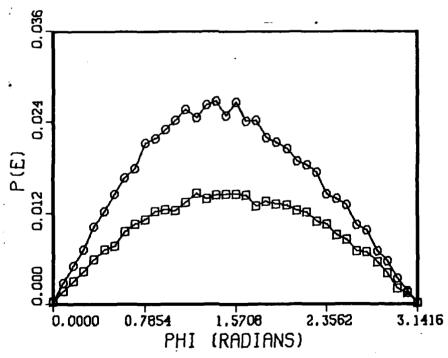Distributions from 2.478E+01 keV Neutron

Fig. C-4 0-50 and 500-550 keV Electron Group Angular
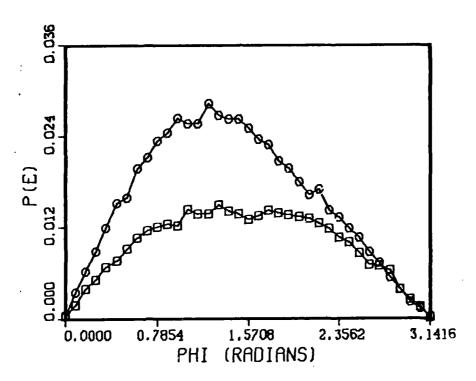Distributions from 5.503E+02 keV Neutron

Fig. C-5   0-50 and 500-550 keV Electron Group Angular
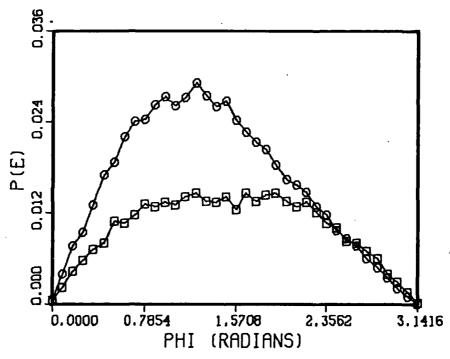Distributions from 2.307E+03 keV Neutron

Fig. C-6   0-50 and 500-550 keV Electron Group Angular
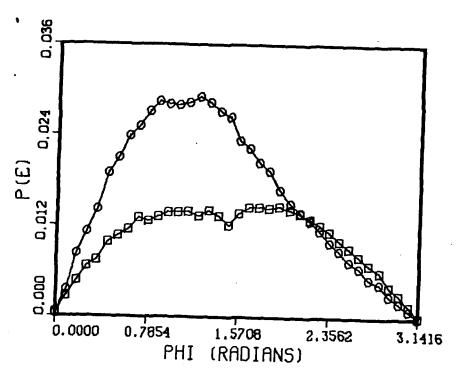Distributions from 4.066E+03 keV Neutron

Fig. C-7 0-50 and 500-550 keV Electron Group Angular
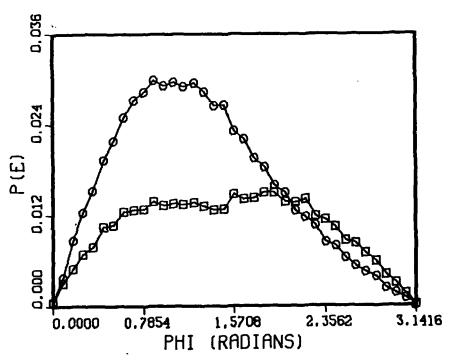Distributions from 6.376E+03 keV Neutron

Fig. C-8 0-50 and 500-550 keV Electron Group Angular
Distributions from 8.187E+03 keV Neutron

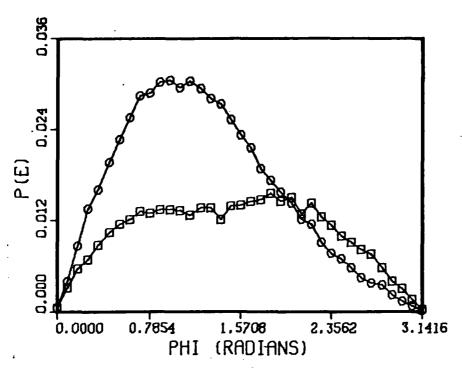Fig. C-9   0-50 and 500-550 Electron Group Angular
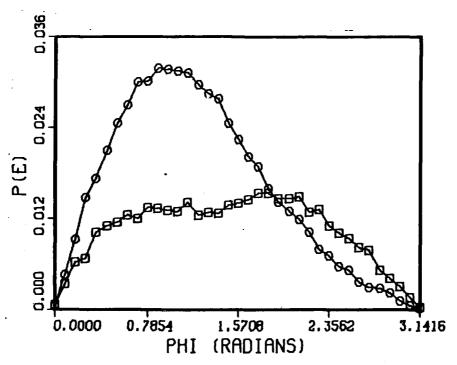Distributions from 1.000E+04 keV Neutron

Fig. C-10   0-50 and 500-550 Electron Group Angular
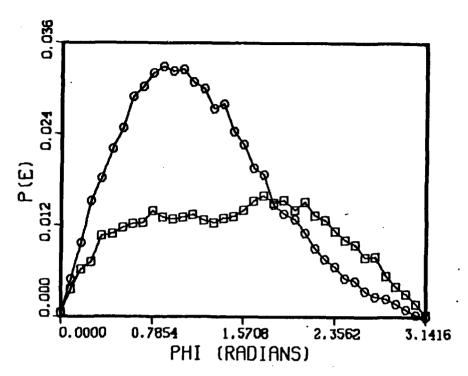Distributions from 1.282E+04 keV Neutron

47

Fig. C-11   0-50 and 500-550 keV Electron Group Angular
Distributions from 1.492E+04 keV Neutron
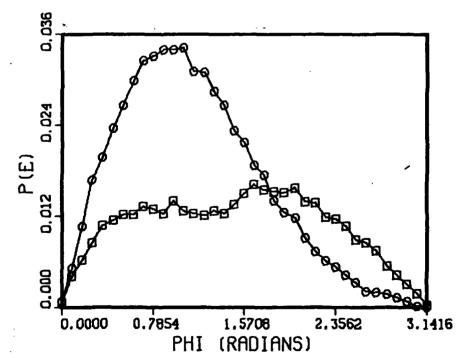
Fig. C-12   0-50 and 500-550 keV Electron Group Angular
Distributions from 1.964E+04 keV Neutron

48

Appendix D

Angular Electron Density Along a Magnetic Field Line

Figure D-1 presents the view of an arbitrary neutron decaying on a magnetic field line. ψ is the angle of incidence of the neutron on the field line. θ is the angle between the neutron velocity vector and the electron velocity vector. And α is the angle between the electron velocity vector and the magnetic field line. The electron distribution as a function of θ is known, however, the electron distribution as a function of α must be found to provide details of the trapped distribution of electrons.
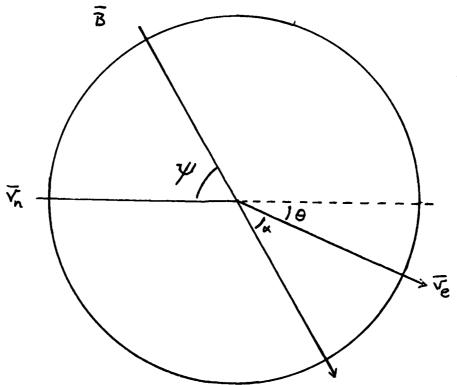
Fig. D-1   Neutron Decay Geometry Around a Magnetic Field Line

Defining α as the angle from the direction of the magnetic
field line, and β as the angle around the base of this vector, two
spherical coordinate frames are defined. To calculate the distribu-
tion of electrons as a function of θ, a coordinate transformation
is required. Figure D-2 shows the relationship between the spherical
coordinate systems. The equations expressing the coordinates in
each frame are:

$$x_1 = r\ \cos\psi\ \sin\theta \qquad\qquad x_1' = \rho\ \cos\beta\ \sin\alpha$$

$$x_2 = r\ \sin\psi\ \sin\theta \qquad\qquad x_2' = \rho\ \sin\beta\ \sin\alpha$$

$$x_3 = r\ \cos\theta \qquad\qquad\qquad x_3' = \rho\ \cos\alpha$$

Fig. D-2 Geometry Axes

The transformation between these coordinate systems is:

$$x_1 = x_1'$$
$$x_2 = x_2'\ \cos\psi\ +\ x_3'\ \sin\psi$$
$$x_3 = -x_2'\ \sin\psi\ +\ x_3'\ \cos\psi$$

These relations result in the relation that,

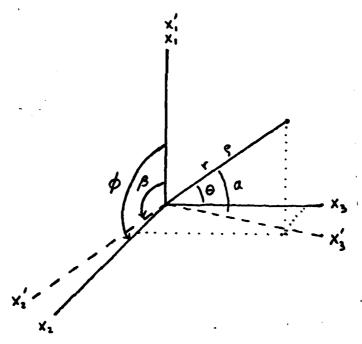$$\cos\theta = -\sin\beta\ \sin\alpha\ \sin\psi + \cos\alpha\ \cos\psi \qquad\qquad (D-1)$$

which, when solved for θ equals,

$$\theta = \text{Arccos}\ (\cos\alpha\ \cos\psi - \sin\beta\ \sin\alpha\ \sin\psi) \qquad\qquad (D-2)$$

For a given α and ψ, the values of θ can be found by iterating β in equation D-2 from $0-2\pi$. Summing the contributions of each electron distribution as a function of θ, each increment can be used to calculate the electron density at that point. The result is the distribution of electrons at an angle α to the magnetic field line.

In this case, where $N(\theta)$ is a polynomial distribution of θ, the number density in $N(\theta)$ must be accounted for by assuming that the electrons are isotropic in ϕ and by dividing $N(\theta)$ by $2\pi\sin\theta$. This calculation determines the number of electrons in an area $d\theta$ by $d\phi$. Since no simple closed form solution of the integrals required to solve this problem exist, the solution must be found numerically as described in the previous paragraph.

Appendix E

User's Manual and Subroutines for
Electron Flux Calculations from Prompt Neutron Spectra

This appendix presents the subroutines added to AFWL's PROMPT radiation code. The subroutine DECAY calculates the electron spectrum and flux from neutron decay. DECAY uses subroutine EMAX to calculate the maximum electron energy from a specific energy neutron. Subroutine RITDK prints the electron spectrum and flux on the output file. Subroutine ANGLE calculates the electron angular distribution as a function of electron energy and angle from the neutron velocity.

DECAY requires a 38 group neutron energy spectrum, array SRSN, as input. It defines its own 50 keV electron energy group spectrum in array EBINN and calculates the electron energy spectrum from the decayed neutrons in array SRSE. The variable EFLUX carries the value of the total electron flux. Besides the neutron source spectrum, no other information is necessary. A listing of the subroutines is provided on the following pages.

Subroutine ANGLE requires the same 38 group neutron energy spectrum and 50 keV electron group as DECAY. The volume of data is large and is written on a dummy tape called TAPE9. A copy of this subroutine is provided after the previous mentioned subroutines.

```
C      SUBROUTINE DECAY(SRSN,SRSE,EFLUX)
C
C      DECAY CALCULATES THE ELECTRON DENSITY DISTRIBUTION
C      FROM THE DECAY OF THE PROMPT NEUTRONS.  REFERENCE TO THE
C      THEORY BEHIND THE FOLLOWING CALCULATIONS IS FOUND IN
C      BRIAN L. HANSON'S THESIS ON THE CONTRIBUTION OF BOMB
C      NEUTRON DECAY TO THE SPACE ELECTRON ENVIRONMENT.
C
C      INPUT PARAMETERS:
C      SRSN.....AN ARRAY CONTAINING THE NEUTRON SOURCE SPECTRUM.
C
C      BINN.....FROM COMMON, THIS ARRAY CONTAINS THE NEUTRON ENERGY
C               BINS CALCULATED IN SUBROUTINE PMPSPC
C      EBINN....FROM COMMON, THIS ARRAY CONTAINS THE ELECTRON ENERGY
C               BINS CALCULATED IN THIS SUBROUTINE.
C
C      OUTPUT PARAMETERS:
C      SRSE.....AN ARRAY CONTAINING THE ELECTRON ENERGY SPECTRUM OF
C               THE ELECTRONS FROM NEUTRON DECAY.
C      EFLUX....THE TOTAL ELECTRON FLUX OBSERVED BY THE SATELLITE.
C
C      DATA VALUES:
C      B......CONTAINS THE ELECTRON ENERGY CURVE FIT CONSTANTS TO
C             CALCULATE THE ELECTRON SPECTRUM FROM ARBITRARY NEUTRON
C             ENERGIES.
C
C      DATE OF SUBROUTINE:     11 DEC 81
C      WRITTEN AND ENTERED BY BRIAN L. HANSON
C
C      DIMENSION SRSN(38),ELECN(38),B(15),SRSE(24)
       COMMON/BIN/ BINN(38),EBINN(24)
       DATA B/ 6.093E-04, 1.076E-08,-3.036E-13, 1.799E-05,
      1-2.364E-10, 5.214E-15,-6.244E-08, 8.373E-13,-1.903E-17,
```

53

```
      2 6.847E-11,-9.915E-16, 2.415E-20,-2.460E-14, 3.797E-19,
      3-9.962E-24/

C     CONSTANT PARAMETERS ARE DEFINED:
C     ENNOT.....NEUTRON REST ENERGY IN KEV.
C     C........SPEED OF LIGHT IN CM/SEC.
C     HLIFE.....THE NEUTRON HALF LIFE OF BETA DECAY.

      ENNOT=939511.
      C=3.000E+10
      PI=3.14159262
      HLIFE=10.6*60.

C     FOR EACH NEUTRON ENERGY GROUP, DEFINE THE NUMBER OF
C     NEUTRONS THAT WOULD DECAY.  RELATIVISTIC TIME DILATION OF
C     THE HALFLIFE AND RELATIVISTIC VELOCITY DISTRIBUTION IS
C     CONSIDERED.

      DO 1 II=1,38
      VELN=SQRT(1.-(1./(1.+(BINN(II)/ENNOT))**2)*C
      HLIFOB=HLIFE/(SQRT(1.-(VELN/C)**2))
      XLAMDA=LOG(2.)/HLIFOB
      TAU=1./XLAMDA
      ELECN(II)=SRSN(II)/(4*PI*VELN*TAU)
    1 CONTINUE

C     INITIALIZE THE ELECTRON SOURCE SPECTUM ARRAY AND DEFINE
C     THE ELECTRON ENERGY BINS IN THE EBINN ARRAY.

      DO 2 II=1,24
      SRSE(II)=0.0
    2 EBINN(II)=50.*(II-1)

C     CALCULATE THE ELECTRON ENERGY DISTRIBUTION PER DECAY NEUTRON
```

54

```
C     FROM THE CURVE FIT DATA.
C
      DO 5 II=1,38
      A0=0.
      A1=0.
      A2=0.
      A3=0.
      A4=0.
C
C     CONVERT BINN ENERGIES IN MEV TO KEV.
C
      E=BINN(II)*1000.
C
C     DETERMINE THE MAXIMUM ELECTRON ENERGY.
C
      CALL EMAX(EEMAX,E)
C
C     CALCULATE THE FOURTH ORDER FIT CONSTANTS FROM THE
C     GIVEN NEUTRON ENERGY.
C
      DO 3 JJ=1,3
      EEN=E**(JJ-1)
      A0=A0+B(JJ)*EEN
      A1=A1+B(JJ+3)*EEN
      A2=A2+B(JJ+6)*EEN
      A3=A3+B(JJ+9)*EEN
      A4=A4+B(JJ+12)*EEN
    3 CONTINUE
C
C     FOR EACH ELECTRON ENERGY BIN, CALCULATE THE CONTRIBUTION
C     EACH DECAYING NEUTRON GIVES TO IT FROM THE FOURTH ORDER CURVE FIT.
C     NUMBER BETWEEN SUCCESSIVE BINS.
C
      PROB2=0.0
```

```fortran
      DO 4 JJ=1,23
      PROB1=PROB2
      E=EBINN(JJ)
      PROB2=A0*E+(A1/2)*E**2+(A2/3)*E**3+(A3/4)*E**4+(A4/5)*E**5
      IF((PROB2.GT.1.).OR.(E.GE.EEMAX)) PROB2=1.0
      PROBE=PROB2-PROB1
      SRSE(JJ)=ELECN(JJ)*PROBE+SRSE(JJ)
    4 CONTINUE
    5 CONTINUE
C
C        INITIALIZE THE FLUX VARIABLES CONTAINING THE ELECTRON
C     FLUX ABOVE 550 KEV (FLX550) AND THE TOTAL ELECTRON FLUX
C     (EFLUX).
C
      FLX550=0.0
      EFLUX=0.0
C
C        FOR EACH ELECTRON ENERGY BIN, CALCULATE THE
C     ELECTRON VELOCITY AND MULTIPLY IT TO THE NUMBER OF
C     ELECTRONS IN THAT ENERGY GROUP.  THE FLUX IS THE
C     SUM OVER ALL GROUPS.
C
C        THE 11TH ARRAY VALUE CONTAINS THE 500-550 ELECTRON
C     ENERGY GROUP.
C
      DO 6 JJ=1,23
      VELE=SQRT(1.-(1./(1.+((EBINN(JJ+1)+EBINN(JJ))/(511.*2.))/(511.*2.))**2))*C
      EFLUX=SRSE(JJ)*VELE+EFLUX
      IF(JJ.GT.11) FLX550=FLX550+VELE*SRSE(JJ)
    6 CONTINUE
C
C        WRITE THE ELECTRON SOURCE SPECTRUM AND THE FLUX
C     DATA ON THE OUTPUT TAPE VIA SUBROUTINE RITDK.
```

56

```
CALL RITDK(SRSE,EFLUX,FLX550)
RETURN
END
```

```
      SUBROUTINE EMAX(EEMAX,ENNEU)

C     EMAX CALCULATES THE MAXIMUM ELECTRON ENERGY
C     A NEUTRON CAN EMIT.

C     INPUT PARAMETERS:
C       ENNEU.....NEUTRON ENERGY IN KEV.
C       EMASS.....ELECTRON REST MASS IN KG.
C       C.........SPEED OF LIGHT IN M/SEC
C       EDECAM....MAX ELECTRON DECAY ENERGY IN KEV FROM A
C                 NEUTRON AT REST.

C     OUTPUT PARAMETERS:
C       EEMAX.....MAXIMUM ELECTRON ENERGY.

C     THIS SUBROUTINE USES THE STRAIGHT FORWARD EMMISSION
C     OF AN ELECTRON FROM A DECAYING NEUTRON.  THE ELECTRON IS
C     ASSUMED TO HAVE THE INITIAL VELOCITY OF THE NEUTRON AND
C     THE ELECTRON VELOCITY FROM THE DECAY ENERGY IS ADDED TO
C     THIS VELOCITY RELATIVISTICALLY.

C     DATE OF SUBROUTINE:   11 DEC 81
C     WRITTEN AND ENTERED BY BRIAN L. HANSON

      EMASS=9.11E-31
      C=3.000E+08
      EDECAM=1.6507*511.
      EMREL=(EDECAM*1.602E-16)/C**2+EMASS
      VELE=SQRT(1.-((EMASS/EMREL)**2))*C
      VELN=SQRT(1.-(1./((ENNEU/939511.)+1.)**2))*C
      VMAX=(VELE+VELN)/(1.+(VELE*VELN/C**2))
      EMREL=EMASS/SQRT(1.0-(VMAX/C)**2)
      EEMAX=(EMREL-EMASS)*C**2/1.602E-16
      RETURN
      END
```

58

```
      SUBROUTINE RITDK(SRSE,EFLUX,FLX550)

C
C     RITDK WRITES THE ELECTRON SPECTRUM FROM THE
C     DECAY NEUTRON SPEC.RUM ON THE OUTPUT FILE.
C     IT ALSO WRITES THE FLUX VALUES ON OUTPUT.
C
C     INPUT PARAMETERS:
C         SRSE.....ELECTRON SPECTRUM FROM DECAYED NEUTRONS.
C         EFLUX....TOTAL ELECTRON FLUX.
C         FLX550...ELECTRON FLUX FOR ELECTON ENERGIES
C                  GREATER THAN 550 KEV.
C
C     OUTPUT:
C         PRINTS ELECTRON SPECTRUM AND FLUXES ON OUTPUT
C         FILE.
C
C     DATE OF SUBROUTINE:      11 DEC 81
C     WRITTEN AND ENTERED BY BRIAN L. HANSON
C
      DIMENSION SRSE(24)
      COMMON/BIN/ BINN(38),EBINN(24)
      WRITE(17,6000)(EBINN(II),SRSE(II),II=1,24)
      WRITE(17,6001)EFLUX
      WRITE(17,6002) FLX550
 6000 FORMAT(1H1,5X,47HTHE ELECTRON ENERGY SPECTRUM FROM NEUTRON DECAY,
     1//,5X,12HENERGY (KEV),5X,15HELECTRONS/CM**3,//,(6X,1PE10.3,
     28X,E10.3))
 6001 FORMAT(////,5X,28HTHE PROMPT ELECTRON FLUX IS ,1PE10.3)
 6002 FORMAT(//,5X,41HTHE ELECTRON FLUX GREATER THAN 550 KEV IS,1PE10.3)
      RETURN
      END
```

59

```fortran
      SUBROUTINE ANGLE(SRSN,SRSE)
      DIMENSION SRSN(38),SRSE(23),F(38)
      DIMENSION FITS(920),AFIT(5),THETA(38),FIT(5)
      COMMON/BIN/ BINN(38),EBINN(23)
      DATA (FITS(I),I=1,40)/6.703E-05,  5.097E-09,  6.954E-12,
     $-2.149E-15,3.166E-19,-2.370E-23, 8.675E-28,-1.233E-32,
     $1.193E-03, 9.247E-07,-4.522E-10, 1.181E-13,
     $1.649E-17, 1.239E-21,-4.719E-26, 7.133E-31,
     $7.822E-05,-1.353E-06, 6.349E-10,-1.652E-13,
     $2.307E-17,-1.735E-21, 6.615E-26,-1.001E-30,
     $3.106E-04, 6.372E-07,-2.897E-10, 7.491E-14,
     $1.044E-04, 7.841E-22,-2.987E-26, 4.517E-31,
     $5.138E-05,-9.617E-08, 4.253E-11,-1.092E-14,
     $1.517E-18,-1.136E-22, 4.317E-27,-6.518E-32/
C
C
C
   50 - 100 KEV FIT DATA
C
C
C
      DATA (FITS(I),I=41,80)/1.539E-04,  1.788E-08,-1.649E-11,
     $4.939E-15,7.099E-19, 5.214E-23,-1.893E-27, 2.699E-32,
     $2.741E-03,-3.136E-07, 1.100E-10,-2.458E-14,
     $2.892E-18,-1.848E-22, 6.120E-27,-8.261E-32,
     $2.545E-04, 3.340E-07,-9.217E-11, 1.599E-14,
     $1.138E-18, 1.884E-23, 1.184E-27,-3.854E-32,
     $7.535E-04,-1.187E-07, 2.856E-11,-3.348E-15,
     $1.536E-19, 5.085E-23,-3.080E-27, 5.917E-32,
     $1.232E-04, 1.387E-08,-3.192E-12, 2.045E-16,
     $7.635E-20,-1.256E-23, 6.789E-28,-1.249E-32/
C
C
C
  100 - 150 KEV FIT DATA
C
C
C
      DATA (FITS(I),I=81,120)/1.699E-04,-2.558E-08, 2.130E-11,
     $-6.589E-15,9.863E-19,-7.566E-23, 2.881E-27,-4.327E-32,
     $3.972E-03,-2.075E-07, 7.759E-11,-1.931E-14,
     $2.511E-18,-1.768E-22, 6.423E-27,-9.392E-32,
```

```
$2.156E-04, 3.318E-07,-1.223E-10, 2.962E-14,
$3.879E-18, 2.790E-22,-1.040E-26, 1.560E-31,
$9.918E-04,-1.617E-07, 4.696E-11,-9.674E-15,
$1.153E-18,-7.898E-23, 2.888E-27,-4.317E-32,
$1.624E-04, 2.531E-08,-5.422E-12, 7.958E-16,
$6.797E-20, 3.499E-24,-1.054E-28, 1.422E-33/
```

C
C   150 - 200 KEV FIT DATA

```
DATA (FITS(I),I=121,160)/9.975E-04,-1.748E-06, 1.116E-09,
$-3.115E-13,4.443E-17,-3.377E-21, 1.299E-25,-1.981E-30,
$4.582E-03,-2.677E-07, 2.190E-10,-6.471E-14,
$9.313E-18,-6.842E-22, 2.467E-26,-3.470E-31,
$4.068E-05, 6.585E-07,-4.478E-10, 1.314E-13,
$1.928E-17, 1.463E-21,-5.498E-26, 8.097E-31,
$9.510E-04,-4.524E-07, 2.856E-10,-8.381E-14,
$1.243E-17,-9.594E-22, 3.680E-26,-5.538E-31,
$1.547E-04, 8.610E-08,-5.256E-11, 1.545E-14,
$2.304E-18, 1.794E-22,-6.949E-27, 1.057E-31/
```

C
C   200 - 250 KEV FIT DATA

```
DATA (FITS(I),I=161,200)/2.427E-04, 2.813E-09, 4.498E-12,
$-6.872E-16,1.209E-20, 7.129E-24,-4.404E-28, 8.529E-33,
$4.548E-03, 5.836E-07,-2.440E-10, 5.538E-14,
$6.318E-18, 3.673E-22,-1.018E-26, 1.026E-31,
$4.859E-04,-6.508E-07, 2.907E-10,-7.045E-14,
$8.624E-18,-5.442E-22, 1.681E-26,-1.992E-31,
$1.278E-03, 1.755E-07,-9.593E-11, 2.586E-14,
$3.428E-18, 2.320E-22,-7.696E-27, 9.895E-32,
$2.064E-04,-8.560E-09, 8.992E-12,-2.909E-15,
$4.264E-19,-3.093E-23, 1.086E-27,-1.473E-32/
```

C
C   250 - 300 KEV FIT DATA

```
C     DATA (FITS(I),I=201,240)/2.325E-04,-2.387E-08, 1.874E-11,
     $-6.193E-15,9.663E-19,-7.640E-23, 2.975E-27,-4.527E-32,
     $4.602E-03, 9.758E-07,-3.903E-10, 9.837E-14,
     $1.398E-17, 1.087E-21,-4.298E-26, 6.713E-31,
     $2.340E-04,-9.767E-07, 3.717E-10,-9.006E-14,
     $1.275E-17,-1.007E-21, 4.059E-26,-6.464E-31,
     $1.135E-03, 2.282E-07,-7.845E-11, 1.716E-14,
     $2.488E-18, 2.125E-22,-9.278E-27, 1.577E-31,
     $1.850E-04,-4.223E-09,-5.344E-13, 6.120E-16,
     $6.586E-20, 5.003E-25, 1.830E-28,-5.754E-33/

C     300 - 350 KEV FIT DATA
C
C     DATA (FITS(I),I=241,280)/2.165E-04, 6.259E-08,-3.629E-11,
     $7.345E-15,6.481E-19, 2.270E-23,-1.753E-29,-1.050E-32,
     $4.377E-03, 8.801E-07,-3.459E-10, 9.356E-14,
     $1.377E-17, 1.087E-21,-4.320E-26, 6.773E-31,
     $1.682E-04,-6.210E-07, 1.631E-10,-3.899E-14,
     $5.419E-18,-4.098E-22, 1.566E-26,-2.367E-31,
     $1.060E-03,-9.393E-08, 1.132E-10,-3.349E-14,
     $4.971E-18,-3.935E-22, 1.577E-26,-2.500E-31,
     $1.752E-04, 6.652E-08,-4.259E-11, 1.195E-14,
     $1.743E-18, 1.363E-22,-5.400E-27, 8.469E-32/

C     350 - 400 KEV FIT DATA
C
C     DATA (FITS(I),I=281,320)/2.100E-04,-1.585E-08, 1.312E-12,
     $2.185E-15,5.991E-19, 6.089E-23,-2.742E-27, 4.596E-32,
     $3.998E-03, 1.276E-06,-4.178E-10, 8.448E-14,
     $9.696E-18, 6.347E-22,-2.211E-26, 3.170E-31,
     $3.548E-05,-1.173E-06, 3.185E-10,-5.853E-14,
     $6.345E-18,-4.049E-22, 1.415E-26,-2.075E-31,
     $8.708E-04, 2.172E-07,-1.209E-11,-4.413E-15,
```

```
      $1.051E-18,-9.028E-23, 3.427E-27,-4.795E-32,
      $1.484E-04, 9.757E-09,-1.540E-11, 4.686E-15,
      $6.700E-19, 4.937E-23,-1.804E-27, 2.584E-32/
C
C     400 - 450 KEV FIT DATA
C
      DATA (FITS(I),I=321,360)/1.556E-04, 6.007E-09, 9.416E-12,
      $-4.432E-15,7.514E-19,-6.106E-23, 2.412E-27,-3.723E-32,
      $2.478E-03, 4.303E-06,-2.500E-09, 6.924E-13,
      $9.855E-17, 7.473E-21,-2.866E-25, 4.359E-30,
      $1.879E-04,-1.995E-06, 1.017E-09,-2.776E-13,
      $3.906E-17,-2.924E-21, 1.107E-25,-1.663E-30,
      $6.526E-04, 6.518E-07,-3.742E-10, 1.046E-13,
      $1.473E-17, 1.095E-21,-4.106E-26, 6.108E-31,
      $1.094E-04,-5.998E-08, 4.251E-11,-1.232E-14,
      $1.734E-18,-1.277E-22, 4.722E-27,-6.921E-32/
C
C     450 - 500 KEV FIT DATA
C
      DATA (FITS(I),I=361,400)/1.402E-04, 2.787E-08,-3.785E-11,
      $1.451E-14,2.453E-18, 2.071E-22,-8.552E-27, 1.372E-31,
      $2.644E-03, 1.917E-06,-7.353E-10, 1.625E-13,
      $1.951E-17, 1.290E-21,-4.415E-26, 6.111E-31,
      $2.121E-04,-2.081E-06, 7.780E-10,-1.679E-13,
      $1.947E-17,-1.235E-21, 4.049E-26,-5.371E-31,
      $6.947E-04, 5.724E-07,-1.873E-10, 3.419E-14,
      $3.052E-18, 1.278E-22,-1.877E-27,-6.500E-33,
      $1.119E-04,-3.248E-08, 4.444E-12, 8.716E-16,
      $3.670E-19, 4.240E-23,-2.061E-27, 3.645E-32/
C
C     500 - 550 KEV FIT DATA
C
      DATA (FITS(I),I=401,440)/1.009E-04,-5.401E-08, 5.191E-11,
      $-1.688E-14,2.586E-18,-2.036E-22, 7.977E-27,-1.229E-31,
```

```
$2.187E-03, 6.172E-07, 9.287E-11,-4.785E-14,
$7.841E-18,-6.466E-22, 2.710E-26,-4.588E-31,
$4.338E-05,-2.122E-06, 1.125E-09,-3.348E-13,
$5.036E-17,-3.949E-21, 1.538E-25,-2.337E-30,
$5.120E-04, 9.623E-07,-6.349E-10, 1.987E-13,
$3.047E-17, 2.418E-21,-9.521E-26, 1.465E-30,
$8.627E-05,-1.093E-07, 8.390E-11,-2.742E-14,
$4.289E-18,-3.446E-22, 1.369E-26,-2.123E-31/

C
C      550 - 600 KEV FIT DATA
C
      DATA (FITS(I),I=441,480)/6.059E-05, 4.164E-08,-2.814E-11,
$7.370E-15,9.526E-19, 6.696E-23,-2.469E-27, 3.724E-32,
$1.838E-03, 1.311E-06,-5.363E-10, 1.411E-13,
$1.988E-17, 1.498E-21,-5.658E-26, 8.354E-31,
$2.570E-04,-1.381E-06, 5.767E-10,-1.567E-13,
$2.241E-17,-1.702E-21, 6.451E-26,-9.510E-31,
$2.429E-04, 3.354E-07,-1.418E-10, 4.229E-14,
$6.367E-18, 4.993E-22,-1.929E-26, 2.865E-31,
$4.269E-05,-8.509E-09, 3.971E-12,-2.167E-15,
$4.054E-19,-3.561E-23, 1.467E-27,-2.250E-32/

C
C      600 - 650 KEV FIT DATA
C
      DATA (FITS(I),I=481,520)/4.438E-05, 1.262E-08, 2.051E-12,
$-2.211E-15,4.480E-19,-4.017E-23, 1.702E-27,-2.768E-32,
$1.248E-03, 1.335E-06,-5.314E-10, 1.316E-13,
$1.780E-17, 1.321E-21,-5.040E-26, 7.685E-31,
$8.622E-05,-1.442E-06, 5.332E-10,-1.285E-13,
$1.717E-17,-1.273E-21, 4.882E-26,-7.504E-31,
$2.253E-04, 4.121E-07,-1.352E-10, 3.164E-14,
$4.203E-18, 3.167E-22,-1.246E-26, 1.970E-31,
$3.930E-05,-2.734E-08, 5.636E-12,-1.124E-15,
$1.457E-19,-1.223E-23, 5.573E-28,-1.006E-32/
```

C
C
C

```
      650 - 700 KEV FIT DATA

      DATA (FITS(I),I=521,560)/3.052E-05,-3.168E-08, 2.960E-11,
     $-9.996E-15,1.642E-18,-1.388E-22, 5.775E-27,-9.342E-32,
     $8.819E-04, 1.271E-06,-5.680E-10, 1.525E-13,
     $2.163E-17, 1.645E-21,-6.338E-26, 9.692E-31,
     $1.765E-04,-1.388E-06, 5.844E-10,-1.552E-13,
     $2.176E-17,-1.637E-21, 6.250E-26,-9.485E-31,
     $8.514E-05, 4.112E-07,-1.588E-10, 4.219E-14,
     $5.872E-18, 4.370E-22,-1.650E-26, 2.479E-31,
     $1.591E-05,-3.023E-08, 8.925E-12,-2.399E-15,
     $3.259E-19,-2.328E-23, 8.395E-28,-1.208E-32/
```

C
C
C

```
      700 - 750 KEV FIT DATA

      DATA (FITS(I),I=561,600)/1.620E-05, 3.828E-08,-3.720E-11,
     $1.261E-14,1.983E-18, 1.587E-22,-6.265E-27, 9.665E-32,
     $4.656E-04, 8.254E-07,-2.540E-10, 5.513E-14,
     $6.677E-18, 4.479E-22,-1.558E-26, 2.189E-31,
     $4.190E-05,-9.150E-07, 2.756E-10,-6.273E-14,
     $7.846E-18,-5.379E-22, 1.898E-26,-2.691E-31,
     $6.149E-05, 2.178E-07,-3.340E-11, 5.849E-15,
     $5.381E-19, 2.381E-23,-3.884E-28,-6.245E-34,
     $1.387E-05,-1.590E-08,-7.708E-13, 3.636E-16,
     $7.114E-20, 6.789E-24,-3.087E-28, 5.339E-33/
```

C
C
C

```
      750 - 800 KEV FIT DATA

      DATA (FITS(I),I=601,640)/1.250E-05,-2.940E-08, 2.858E-11,
     $-8.825E-15,1.268E-18,-9.308E-23, 3.397E-27,-4.889E-32,
     $1.630E-04, 8.757E-07,-4.036E-10, 1.088E-13,
     $1.518E-17, 1.130E-21,-4.258E-26, 6.377E-31,
     $9.426E-05,-7.408E-07, 2.865E-10,-7.884E-14,
```

65

```
$1.119E-17,-8.421E-22, 3.197E-26,-4.810E-31,
$8.858E-06, 2.036E-07,-6.237E-11, 1.856E-14,
$2.750E-18, 2.118E-22,-8.139E-27, 1.232E-31,
$1.519E-06,-1.201E-08, 2.808E-13,-4.808E-16,
$1.006E-19,-8.857E-24, 3.615E-28,-5.611E-33/

C
C       800 - 850 KEV FIT DATA
C

      DATA (FITS(I),I=641,680)/5.787E-06, 1.388E-08,-1.405E-11,
$5.166E-15,8.416E-19, 6.861E-23,-2.741E-27, 4.270E-32,
$7.982E-05, 4.037E-07,-1.268E-10, 2.933E-14,
$3.702E-18, 2.556E-22,-9.078E-27, 1.295E-31,
$3.296E-05,-4.933E-07, 1.457E-10,-3.481E-14,
$4.516E-18,-3.179E-22, 1.143E-26,-1.644E-31,
$2.119E-06, 1.674E-07,-3.558E-11, 8.019E-15,
$1.001E-18, 6.752E-23,-2.312E-27, 3.150E-32,
$2.354E-09,-1.628E-08, 6.909E-13,-2.788E-18,
$1.291E-20, 1.843E-24,-1.018E-28, 1.986E-33/

C
C       850 - 900 KEV FIT DATA
C

      DATA (FITS(I),I=681,720)/2.608E-07, 4.414E-09, 2.311E-12,
$-1.387E-15,2.676E-19,-2.300E-23, 9.165E-28,-1.384E-32,
$1.703E-06, 4.161E-08, 5.256E-11,-1.502E-14,
$1.903E-18,-1.221E-22, 3.871E-27,-4.796E-32,
$1.836E-06,-5.699E-08,-8.260E-11, 2.497E-14,
$3.373E-18, 2.315E-22,-7.868E-27, 1.050E-31,
$6.996E-07, 2.391E-08, 3.971E-11,-1.228E-14,
$1.706E-18,-1.206E-22, 4.223E-27,-5.816E-32,
$8.886E-08,-3.247E-09,-6.002E-12, 1.873E-15,
$2.632E-19, 1.882E-23,-6.662E-28, 9.262E-33/

C
C       900 - 950 KEV FIT DATA
C
```

```
      DATA (FITS(I),I=721,760)/3.854E-07,-8.517E-09, 9.721E-12,
     $-3.090E-15,4.916E-19,-4.138E-23, 1.744E-27,-2.875E-32,
     $7.139E-07,-8.815E-09,-7.800E-13, 4.268E-15,
     $8.912E-19, 8.216E-23,-3.625E-27, 6.169E-32,
     $1.835E-06, 3.002E-08,-1.787E-11,-3.574E-16,
     $4.022E-19,-4.687E-23, 2.297E-27,-4.175E-32,
     $1.017E-06,-1.745E-08, 1.214E-     -1.006E-15,
     $1.184E-20, 7.915E-24,-5.123E.2  1.062E-32,
     $1.662E-07, 2.912E-09,-2.146E .2, 2.518E-16,
     $1.310E-20,-2.898E-26, 3.117E-29,-8.792E-34/

C       950 - 1000 KEV FIT DATA
C
C
      DATA (FITS(I),I=761,800)/1.326E-07, 2.802E-09,-3.153E-12,
     $1.089E-15,1.461E-19, 9.285E-24,-2.730E-28, 2.874E-33,
     $6.075E-07,-1.515E-08, 2.085E-11,-9.293E-15,
     $1.776E-18,-1.619E-22, 7.059E-27,-1.180E-31,
     $6.643E-07, 1.764E-08,-2.575E-11, 1.211E-14,
     $2.434E-18, 2.298E-22,-1.027E-26, 1.750E-31,
     $2.680E-07,-7.416E-09, 1.120E-11,-5.414E-15,
     $1.114E-18,-1.068E-22, 4.826E-27,-8.283E-32,
     $3.639E-08, 1.038E-09,-1.605E-12, 7.905E-16,
     $1.651E-19, 1.597E-23,-7.258E-28, 1.251E-32/

C       1000 - 1050 KEV FIT DATA
C
C
      DATA (FITS(I),I=801,840)/3.923E-08, 9.130E-10,-1.220E-12,
     $5.600E-16,1.174E-19, 1.210E-23,-5.831E-28, 1.049E-32,
     $4.541E-08, 1.048E-09,-1.319E-12, 5.319E-16,
     $8.891E-20, 6.448E-24,-1.874E-28, 1.538E-33,
     $1.448E-07,-3.359E-09, 4.365E-12,-1.890E-15,
     $3.611E-19,-3.300E-23, 1.399E-27,-2.231E-32,
     $8.310E-08, 1.930E-09,-2.519E-12, 1.102E-15,
     $2.139E-19, 2.000E-23,-8.712E-28, 1.429E-32,
```

67

```
$1.382E-08,-3.212E-10, 4.202E-13,-1.845E-16,
$3.606E-20,-3.402E-24, 1.498E-28,-2.482E-33/

C
C
        1050 - 1100 KEV FIT DATA

      DATA (FITS(I),I=841,880)/1.166E-10,-8.545E-12, 1.944E-14,
     $-1.251E-17,3.392E-21,-4.325E-25, 2.500E-29,-5.010E-34,
     $9.344E-09,-2.004E-10, 2.405E-13,-9.642E-17,
     $1.691E-20,-1.387E-24, 5.029E-29,-6.353E-34,
     $1.530E-08, 3.400E-10,-4.263E-13, 1.802E-16,
     $3.398E-20, 3.094E-24,-1.308E-28, 2.026E-33,
     $7.641E-09,-1.718E-10, 2.183E-13,-9.373E-17,
     $1.802E-20,-1.683E-24, 7.345E-29,-1.178E-33,
     $1.198E-09, 2.711E-11,-3.467E-14, 1.499E-17,
     $2.909E-21, 2.749E-25,-1.216E-29, 1.981E-34/

C
C
        1100 - 1150 KEV FIT DATA

      DATA (FITS(I),I=881,920)/1.762E-10, 4.283E-12,-5.929E-15,
     $2.801E-18,6.058E-22, 6.571E-26,-3.475E-30, 7.126E-35,
     $3.903E-10,-9.489E-12, 1.313E-14,-6.205E-18,
     $1.342E-21,-1.456E-25, 7.699E-30,-1.579E-34,
     $2.876E-10, 6.992E-12,-9.678E-15, 4.572E-18,
     $9.889E-22, 1.073E-25,-5.673E-30, 1.163E-34,
     $8.620E-11,-2.096E-12, 2.901E-15,-1.370E-18,
     $2.964E-22,-3.215E-26, 1.700E-30,-3.486E-35,
     $9.033E-12, 2.196E-13,-3.040E-16, 1.436E-19,
     $3.106E-23, 3.369E-27,-1.782E-31, 3.653E-36/

C
C
        DEFINE THE ANGULAR BIN VALUES FROM 0 TO 180
C       DEGREES IN RADIANS.
C
        THETA(1)=(-2.5/180.)*3.1415926
        DO 7 II=2,38
```

68

```fortran
      THETA(II)=(5./180.)*3.1415926+THETA(II-1)
    7 CONTINUE
C
C     DEFINE THE INITIAL ARRAY DIMENSIONS
C
      THETA(1)=0.0
      NTHETA=38
C
C     EXPECTED ANGULAR DISTRIBUTION FOR THOSE ELECTRONS.
C
      DO 9 II=1,NTHETA
    9 P(II)=0.0
C
C     FOR EACH ELECTRON ENERGY GROUP FOR EACH
C     NEUTRON ENERGY GROUP, CALCULATE THE ANGULAR
C     DISTRIBUTION OF EACH ELECTRON ENERGY GROUP.
C
      DO 3 JJ=1,23
C
C     FIND THE FIVE FIT CONSTANTS FROM THE DATA
C
C.....THE ARRAY DIMENSION OF FITS FOR THE
C     BEGINNING OF THE FIT COEFFICIENTS.
C
      N=(8*JJ)-7
      DO 6 I=1,8
    6 FIT(I)=FITS(N-1+I)
C
C     FOR EACH NEUTRON ENERGY GROUP, FIND THE
C     APPROPRIATE FIT CONSTANTS AND SUM OVER EACH
C     NEUTRON ENERGY GROUP, THE ELECTRON DISTRIBUTION.
C
      DO 8 K=1,38
      DO 1 II=1,5
```

```
      A=0.
      EN=BINN(K)
      DO 2 JK=1,8
      E=EN**(JK-1)
      A=A+FIT(JK)*E
    2 CONTINUE
      AFIT(II)=A/(3.14159262*5./180.)
    1 CONTINUE
C
C         AFIT CONTAINS THE 4TH ORDER CURVE FIT
C     CONSTANTS FOR THE ANGULAR DISTRIBUTION OF
C     DECAY ELECTRON ENERGIES.
C
      DO 4 I=1,NTHETA
      IF(THETA(I).EQ.0.) THETA(I)=1.E-30
      DIST=0.0
      DO 5 II=1,5
      THTA=THETA(I)**(II-1)
      DIST=AFIT(II)*THTA+DIST
    5 CONTINUE
      P(I)=P(I)+DIST
    4 CONTINUE
    8 CONTINUE
      WRITE(9)(P(I),I=1,NTHETA)
    3 CONTINUE
      RETURN
      END
```

VITA

Brian L. Hanson was born on 5 January 1956 in Inglewood,
California. He graduated from high school in Oak Harbor, Washington
in 1974 and attended the United States Air Force Academy in Colorado
Springs, Colorado where he received the degree of Bachelor of Science
in Mathematics in May 1978. Upon graduation he was commissioned a
2Lt in the United States Air Force where he was assigned to the
Satellite and C^3 Branch, Environments Section, at the Air Force
Weapons Laboratory on Kirtland Air Force Base in New Mexico. He
worked at Kirtland until he entered the School of Engineering,
Air Force Institute of Technology, in August 1981. He is a member
of the American Nuclear Society and the American Association for the
Advancement of Science.

Permanent address: Oak Harbor, Washington 98277

REPORT DOCUMENTATION PAGE		READ INSTRUCTIONS BEFORE COMPLETING FORM
1. REPORT NUMBER AFIT/GNE/PH/82-8	**2. GOVT ACCESSION NO.** AD-A115 512	**3. RECIPIENT'S CATALOG NUMBER**
4. TITLE (and Subtitle) NEUTRON DECAY ELECTRON INJECTION INTO THE MAGNETOSPHERE		**5. TYPE OF REPORT & PERIOD COVERED** MS Thesis
		6. PERFORMING ORG. REPORT NUMBER
7. AUTHOR(s) Brian L. Hanson 1Lt, USAF		**8. CONTRACT OR GRANT NUMBER(s)**
9. PERFORMING ORGANIZATION NAME AND ADDRESS Air Force Institute of Technology (AFIT-EN) Wright-Patterson AFB, Ohio 45433		**10. PROGRAM ELEMENT, PROJECT, TASK AREA & WORK UNIT NUMBERS**
11. CONTROLLING OFFICE NAME AND ADDRESS		**12. REPORT DATE** March 1982
		13. NUMBER OF PAGES 81
14. MONITORING AGENCY NAME & ADDRESS(if different from Controlling Office)		**15. SECURITY CLASS. (of this report)** Unclassified
		15a. DECLASSIFICATION/DOWNGRADING SCHEDULE

16. DISTRIBUTION STATEMENT (of this Report)

Appropriate for public release; distribution unlimited.

17. DISTRIBUTION STATEMENT (of the abstract entered in Block 20, if different from Report)

18. SUPPLEMENTARY NOTES

Approved for public release; IAW AFR 190-17

15 APR 1982

Dean for Research and Professional Development
Air Force Institute of Technology (ATC)
Wright-Patterson AFB, OH 45433

19. KEY WORDS (Continue on reverse side if necessary and identify by block number)

Electron Injection
Neutron Decay
High Altitude Nuclear Environment
Satellite Survivability/Vulnerability

20. ABSTRACT (Continue on reverse side if necessary and identify by block number)
    A model to determine magnetospheric electron fluxes from bomb neutron decay is presented. The source of electrons is determined from a neutron decay model dependent on a 37 group neutron spectrum of a nuclear detonation. Monte-carlo simulation of the decay process determined the electron energy and angular spectra as a function of neutron energy. The Air Force Weapons Laboratory's PROMPT code generates neutron spectra from a nuclear detonation seen any place above the horizon. Using this neutron spectrum and the electron energy and angular distributions from neutron decay theory, an

DD FORM 1 JAN 73 **1473**   EDITION OF 1 NOV 65 IS OBSOLETE

20. (cont'd)

algorithm was developed to calculate the electron flux. An example of a 1 kiloton burst at 20 km shows that fluxes above normal background can be observed as far away as 400 km. Higher bursts or bursts of larger magnitudes will produce higher fluxes at this distance. It is thus concluded that neutron decay alone can generate significant numbers of energetic electrons in the magnetosphere. Their effect may prove to be of tactical significance in medium to high altitude burst scenarios where fission debris is a less significant source of electrons.